Materials Research Express

INCLUSIVE PUBLISHING
TRUSTED SCIENCE

PAPER • **OPEN ACCESS**

Electrodeposition of Zn/TiO_2 coatings on Ti_6Al_4V produced by selective laser melting, the characterization and corrosion resistance

To cite this article: Demet Özaydın Gündüz *et al* 2024 *Mater. Res. Express* **11** 066522

View the article online for updates and enhancements.

You may also like

- PHOTOMETRIC ANALYSIS OF OVERCONTACT BINARIES AK HER, HI DRA, V1128 TAU, AND V2612 OPH
. Çalkan, O. Latkovi, G. Djuraševi et al.
- Eco-Friendly Synthesis and Characterization of Reduced Graphene Oxide
D. Ickecan, R Zan and S. Nezir
- Design of a gust generator and comparison of model wind turbine and porous disc wake flows in a transverse gust
I. Yigili, M. A. Andirin, M. T. Akpolat et al.



This content was downloaded from IP address 194.27.6.19 on 22/07/2024 at 23:08

Materials Research Express

PAPER

Electrodeposition of Zn/TiO_2 coatings on Ti_6Al_4V produced by selective laser melting, the characterization and corrosion resistance

Demet Özaydın Gündüz[1], **Gökhan Küçüktürk**[1,*], **Muharrem Pul**[2], **Sachin Salunkhe**[1], **Duran Kaya**[3], **Mehmet Kabalcı**[4], **Robert Čep**[5] **and Emad Abouel Nasr**[6]

[1] Gazi University, Faculty of Engineering, Department of Mechanical Engineering, Ankara, Turkey
[2] Department of Electricity and Energy, Kırıkkale Vocational School, Kırıkkale University, Kırıkkale, Turkey
[3] Gazi University Project Coordination Implementation and Research Center, Ankara, Turkey
[4] Kırıkkale University, Faculty of Medicine, Department of Cardiovascular Surgery, Kırıkkale, Turkey
[5] Department of Machining, Assembly and Engineering Metrology, Faculty of Mechanical Engineering, VSB-Technical University of Ostrava, 17. Listopadu 2172/15, 708 00, Ostrava, Czech Republic
[6] Department of Industrial Engineering, College of Engineering, King Saud University, PO Box 800, Riyadh, 11421, Saudi Arabia
[*] Author to whom any correspondence should be addressed.

E-mail: demetozaydin@gazi.edu.tr, gkucukturk@gazi.edu.tr, mpul@kku.edu.tr, sachinsalunkhe@gazi.edu.tr, durankaya@gazi.edu.tr, kabalci@hotmail.com, robert.cep@vsb.cz and eabdelghany@ksu.edu.sa

Keywords: electrodepositions, Zn, doped, TiO_2, coatings, Ti_6Al_4V

OPEN ACCESS

RECEIVED
15 February 2024

REVISED
7 April 2024

ACCEPTED FOR PUBLICATION
19 June 2024

PUBLISHED
28 June 2024

Original content from this work may be used under the terms of the Creative Commons Attribution 4.0 licence.

Any further distribution of this work must maintain attribution to the author(s) and the title of the work, journal citation and DOI.

Abstract

Recently, additive manufacturing techniques have begun to be implemented extensively in the production of implants. Ti6Al4V alloy is a material of choice for implants due to its low density and high biocompatibility. Recent research, however, has demonstrated that Ti6Al4V alloy emits long-term ions (such as Al and V) that are hazardous to health. Surface modifications, including coating, are therefore required for implants. The electrodeposition method was utilized to deposit Zn-doped TiO_2 onto the surfaces of Ti6Al4V samples, which were manufactured via the selective laser melting method. The effects of processing time, amount of TiO_2 addition, microstructure of anode materials, and resistance to wear and corrosion were investigated. The coating hardness and thickness increased with increasing processing time and TiO_2 concentration. It has been observed that the addition of TiO_2 to zinc anode coatings results in an increase in wear and a decrease in corrosion rate. It was noted that the specimens exhibiting the most significant wear also possessed the highest hardness value. The specimens were generated utilizing a graphite anode, underwent a 30-min processing time, and comprised 10 g l^{-1} of TiO_2.

1. Introduction

Implant construction is the primary application of biomedical materials in numerous fields, including orthopaedics, dentistry, drug delivery, and tissue engineering. In order to be deemed suitable for implantation, a material must demonstrate that it is devoid of any detrimental biological effects and is compatible with the functioning of the human body [1, 2].

Musculoskeletal system implants frequently incorporate titanium and its alloys due to their superior biomechanical and biochemical compatibility compared to alternative metallic materials like stainless steel and Co-based alloys [2, 3]. Although Ti alloys possess the most desirable properties, they can prolong the manufacturing process of complex geometry components like bone implants. Additive manufacturing (AM) methodologies have recently been implemented to fabricate metallic components featuring elaborate geometric intricacies. Additive manufacturing (AM), or rapid prototyping (RP), encompasses all technologies that utilize layer-by-layer material fabrication to create end-use components with the necessary industrially acceptable properties. Unlike conventional manufacturing processes, the AM method enables the fabrication of parts that closely resemble the net shape without rough machining [4, 5].

© 2024 The Author(s). Published by IOP Publishing Ltd

Table 1. Chemical composition of Ti6Al4V Grade 5 ELI.

Ti	Al	V	O	N	C	H	Fe
Bal.	5.5–6.75	3.5–4.5	< 0.13	< 0.05	< 0.08	< 0.012	< 0.25

Selective laser melting (SLM) is an additive manufacturing (AM) technique that utilizes computer-controlled focused laser scanning of a metallic powder bed to generate three-dimensional, nearly net-shaped components [5]. SLM is one of the techniques that has gained widespread medical application in recent years, particularly in the prosthetic knee and hip implant industries, which manufacture bone implants. Research on the microstructure and mechanical properties of SLM-produced titanium alloys reveals that these exhibit enhanced hardness and tensile strength compared to conventionally machined and cast products. As mentioned earlier, the circumstance is linked to developing the (α') HCP martensite phase and epitaxial growth [6].

It has been noted that prolonged corrosion of the Ti6Al4V alloy, utilized in fabricating a diverse range of implants owing to its exceptional mechanical properties, can result in adverse biological effects or even allergic reactions due to the liberation of metal ions. Vanadium (V) in the Ti6Al4V alloy has been identified as potentially cytotoxic and capable of inducing long-term adverse reactions in body tissues; aluminum (Al) is associated with neurological disorders, including Alzheimer's [7, 8].

To improve the properties of implant submaterials, various surface modifications are applied with physical modifications such as laser texturing [9] and different coating methods such as pulsed laser coating [10], PVD [11] and pulsed electrochemical coating [12]. Of these modifications, the coating process is a preferred method for developing properties such as desired biocompatibility, fatigue resistance, corrosion resistance, prevention of bone and soft tissue adhesion (osteoconduction) and surface hardness, as it can be applied with many different techniques [13]. One of the most important features of electrophoretic coating, which is one of the coating techniques, is that particles suspended in the liquid medium can be coated. Electrophoretic deposition (EPD) is a highly preferred method for producing bioactive coatings on complex form substrates due to its ability to deposit at ambient temperature. The EPD method offers several advantages, including its versatile application, simple device and equipment requirement, short processing time, cost-effectiveness, ease of modification, and the ability to accumulate particles at the desired density in the final product [14, 15].

Although numerous studies have used other antibacterial elements with antimicrobial properties, such as Ag and Cu, their potential cytotoxicity is still a concern. Zinc is a vital trace element that serves essential functions in the human body, such as DNA synthesis, enzyme activity and cell division. Various studies have reported that Zn can increase cytocompatibility [16] and exhibit antibacterial activity [17]. In recent times, there have been reports indicating that Zn ions can effectively impede bacterial growth and reduce bacterial adhesion and growth. A primary advantage of safeguarding metal surfaces with Zn/Zn alloy coating is providing a cathodic corrosion protection layer. This layer effectively prevents and impedes the corrosive environment from compromising the substrate material for an extended period [18]. The Ti6Al4V surface was coated with Zn-doped ZrO_2/TiO_2 porous coatings (Zn-ZrO_2/TiO_2) by Wang *et al* utilizing a hybrid technique consisting of magnetron sputtering and micro-arc oxidation. It was discovered to possess remarkable antibacterial properties against *S. aureus* and an acceptable level of cytotoxicity. Additionally, they underscored the extent of compatibility [19, 20]. Using the electrodeposition method, He *et al* produced a superhydrophobic surface with a $Zn/ZnO/TiO_2$ coating on Ti6Al4V alloy in their study. Mirak *et al* deposited biocompatible zinc-hydroxyapatite-titania and zinc-hydroxyapatite nanocomposite coatings onto NiTi shape memory alloy using electrodeposition. In comparison to Zn-HA and bare NiTi, Zn-HA/TiO_2 composite coatings exhibited the highest corrosion resistance, according to the authors [21].

This research aimed to safeguard the primary metal of a custom-made implant against corrosion caused by bodily fluids. In light of this rationale, Ti6Al4V components manufactured by SLM were coated with Zn-doped TiO_2 via the EPD method. Various counter electrodes were employed at different concentrations and times.

2. Materials and methods

2.1. Sample preparation and electrodeposition coating

The Ti6Al4V Grade 5 ELI samples, produced by selective laser melting (SLM), were used as the substrate. The chemical composition of Ti6Al4V Grade 5 ELI is given in table 1. SLM process was performed with Ermaksan ENA Vision 250 SLE device using 0.085 laser diameter, 1000 mm s^{-1} laser speed, 280 W Laser power, and 0.120 Hatch distance parameters.

Table 2. Electrolyte composition and process conditions [22].

Electrolyte composition	Concentration (g/l)	Parameters
$ZnCl_2$ _	75	current density: 4 A/ ^{dm2}
KCl	230	temperature: 25±2 °C
H3BO3	20	pH: 5,9±0,2
TiO_2 particle _	5 and 10	Mixing speed:200 rpm

Table 3. Treatment groups and sample numbering.

Sample No.	TiO_2 addition amount	Processing time (min.)	Anode material
G30(5)	5 g l^{-1}	30	
G60(5)	5 g l^{-1}	60	
G30(10)	10 g l^{-1}	30	Graphite
G60(10)	10 g l^{-1}	60	
Z30(5)	5 g l^{-1}	30	
Z60(5)	5 g l^{-1}	60	
Z30(10)	10 g l^{-1}	30	Zinc
Z60(10)	10 g l^{-1}	60	

Samples with dimensions of 20 × 20 × 3.5 cm were cut from the sheets produced by SLM with a precision cutting device. After the cut samples were sanded with 220 and 400-grit mesh sandpaper, the surface was washed with alcohol.

The electrochemical solution given in table 2 was used for the electrodeposition process. According to the process groups shown in table 3, the EPD process was carried out at two different times, 30 and 60 min, with the addition of two different TiO_2 (anatase,∼ 325 mesh, ⩾99%) 5 g l^{-1} and 10 g l^{-1}. Additionally, to compare the TiO_2 accumulation change, coating processes were carried out with graphite and pure (99.9%) Zn counter electrode.

2.2. Characterization of implant material surfaces

The coating thickness of the electrophoretic deposition (EPD) applied samples was measured using a Leica Microsystems optical microscope. Pre- and post-*in vitro* corrosion process examinations of the EPD-applied samples were conducted through SEM and EDS analyses. The analyses were performed with a field emission scanning electron microscope, specifically the HITACHI SU5000 (FE-SEM).

Micro-hardness Analysis: Vickers microhardness measurements were conducted using a Highwood HWMMT-X3 hardness device. In the test, a 50-gf load was applied for 10 s.

In vitro corrosion tests: The corrosion behaviour was assessed in commercial Hank's Balanced Salt Solution (Biowest X0510 HBSS 10X without Calcium, without Magnesium, with Sodium Bicarbonate, without Phenol Red) at room temperature. The working cell was equipped with three standard electrodes: Pt as the counter electrode, a common calomel electrode as the reference electrode, and the working electrode. Subsequently, the samples were immersed in the solution, and an open circuit potential (OCP) was applied for 30 min. The data was obtained by covering the potential from − 0.25 V versus OCP to 0.25 V. The scan rate was 0.17 mV s^{-1}. The graphs calculated corrosion current density (i_{corr}) and corrosion potential from the extrapolated points where the anodic and cathodic overpotentials were about ±50 mV.

Wear resistance test: The wear test was conducted using a pin-on-plate test system, applying a load of 15 kg at a speed of 80 mm s^{-1} for 900 s. The counter abrasive was a 5 mm diameter bearing ball made of 100Cr6 material. Wear amounts were compared using the weight difference method. Weight difference measurements were made with a precision scale.

3. Results and discussion

3.1. Surface morphology

SEM images of Zn-doped TiO_2 coatings on a Ti6Al4V alloy substrate manufactured using SLM are shown in figure 1. The figures serve to emphasize the porous composition of the coating. It is apparent from the SEM images in the figure that the surface structure transforms the concentration of TiO_2 increases from 5 g l^{-1} to 10 g l^{-1}.

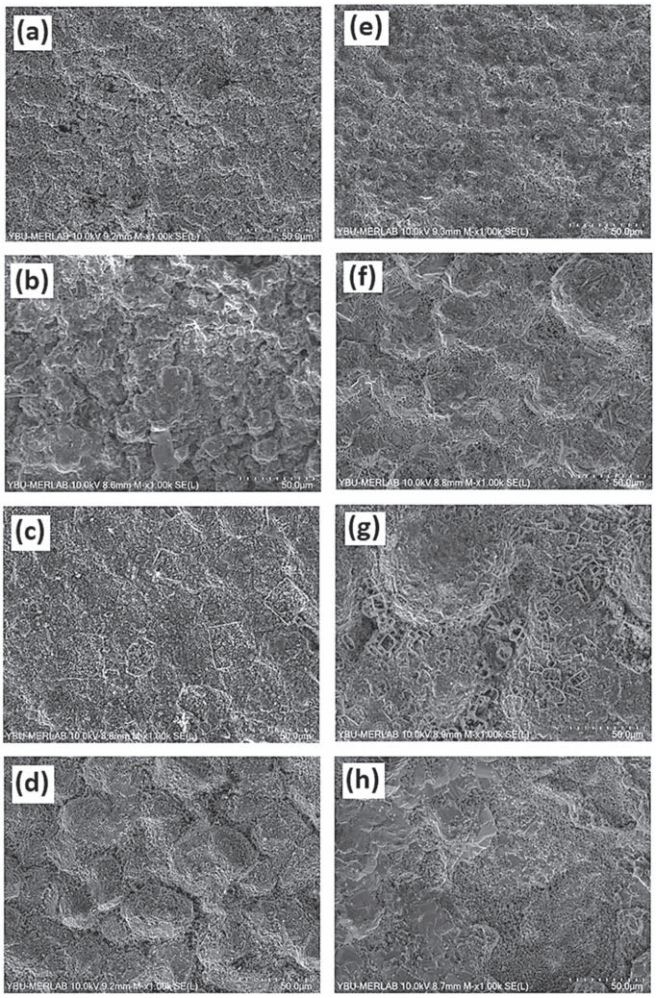


Figure 1. SEM images of Zn-doped TiO_2 coatings on Ti6Al4V alloy substrate produced using SLM (a) G30-5, (b) G60-5, (c) G30-10, (d) G60-10, (e) Z30-5, (f) Z60-5, (g) Z30-10, (h) Z60-10.

A discernible alteration in surface morphology ensues from the augmentation of TiO_2 quantity, which possesses a ceramic and exceedingly rigid phase, coupled with the extension of the processing time from 30 min to 60 min. Surface roughness increases when examining SEM images, primarily due to doubling the processing time. The SEM images indicate that surface morphology varies between processes utilizing the same amount and duration of TiO_2. Graphite and zinc anodes are nonetheless utilized independently.

In order to determine how the elemental distribution reflected the various surface morphologies observed in SEM images, EDS analyses were conducted on every experimental sample. EDS mapping and exploring SEM images of G60-10 and Z60-10 samples with the greatest processing time and TiO_2 quantity are depicted in figure 2. The cumulative results of the EDS analyses performed on all test samples are presented in table 4.

Figure 2 further discerns that the morphology comprises plate-like regions, some of which extend outward, consistent with the findings of Guan *et al* [23]. Sajjadnejad *et al* reported that particles within the Zn matrix close active defect areas (such as pores, voids, micro-holes, crevices, etc) against corrosion, forming a compact layer with a protective function [24]. Similarly, SEM images reveal the accumulation of TiO_2 particles in the intermediate regions.

Table 4 indicates that sample Z60(10) exhibited the highest accumulation of TiO_2, whereas sample G60(10) showed the lowest TiO_2 accumulation. Notably, for electrodeposition coatings produced using the graphite anode, a decreasing trend is observed in the amount of additional TiO_2 property units for the same processing time. Moreover, within coatings created with graphite anode, an augmentation in the accumulation of Zn on the surface is noted with increased processing time and the quantity of additional TiO_2 particles in the solution. Conversely, coatings manufactured with a Zn anode demonstrate a decrease in the amount of Zn accumulated on the surface as both processing time and the quantity of additional TiO_2 particles increase. Tuaweri *et al* investigated the impact of applied current density, deposition time, particle concentration, and agitation on the current efficiency and deposition characteristics of Zn-SiO_2 composite coatings. Their findings revealed that,

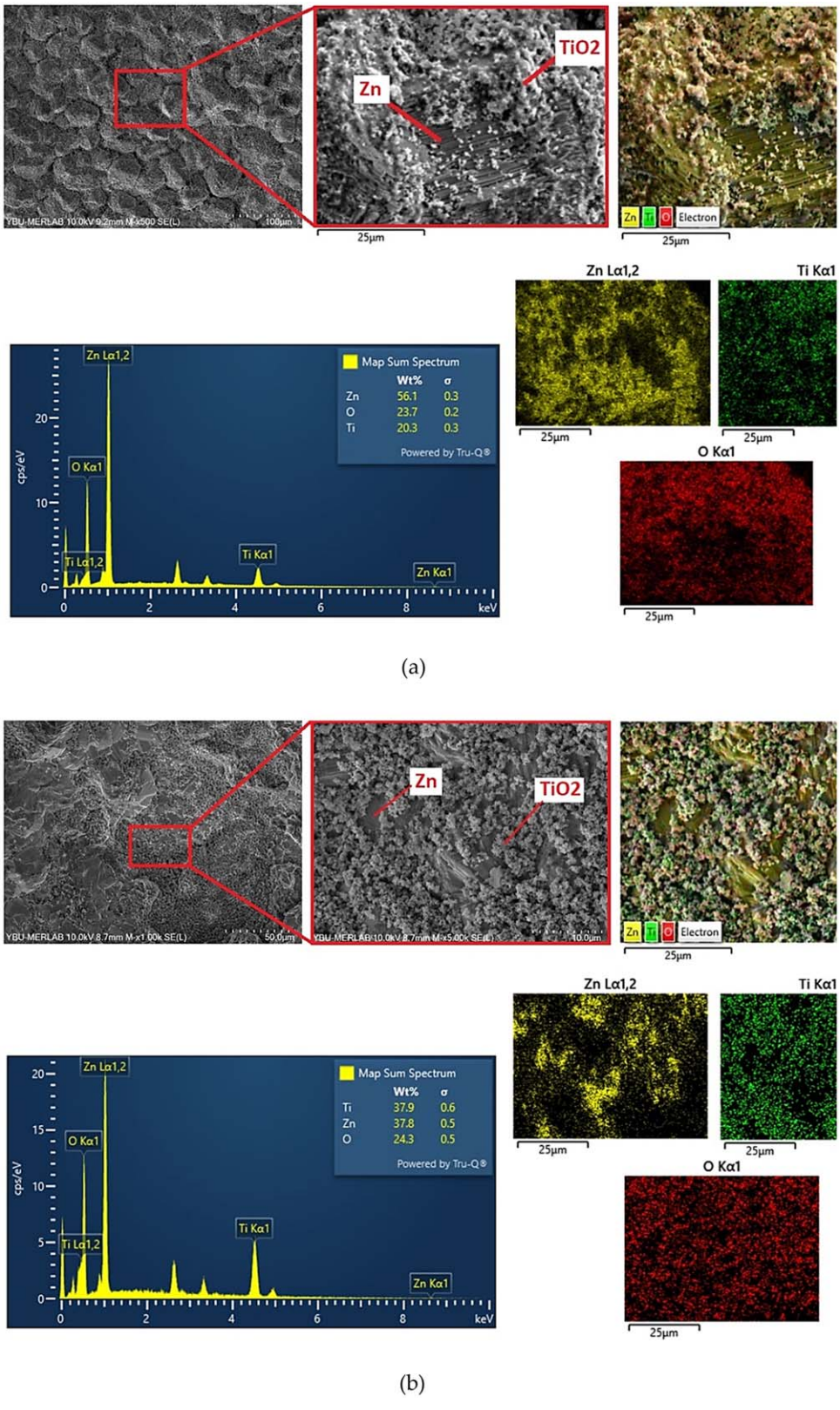


Figure 2. SEM images and Element distribution maps of graphite anode (a) G60-10 and zinc anode (b) Z60-10.

over time, Zn dendrites encountered challenges in accumulating through the dense SiO_2 layer. In Zn anode coatings, the observed decrease in the accumulation of Zn on the surface, correlated with increased processing time and additional TiO_2 particle concentration, can be attributed to the electrochemical accumulation mechanism of zinc, as elucidated by Tuaweri *et al* [25].

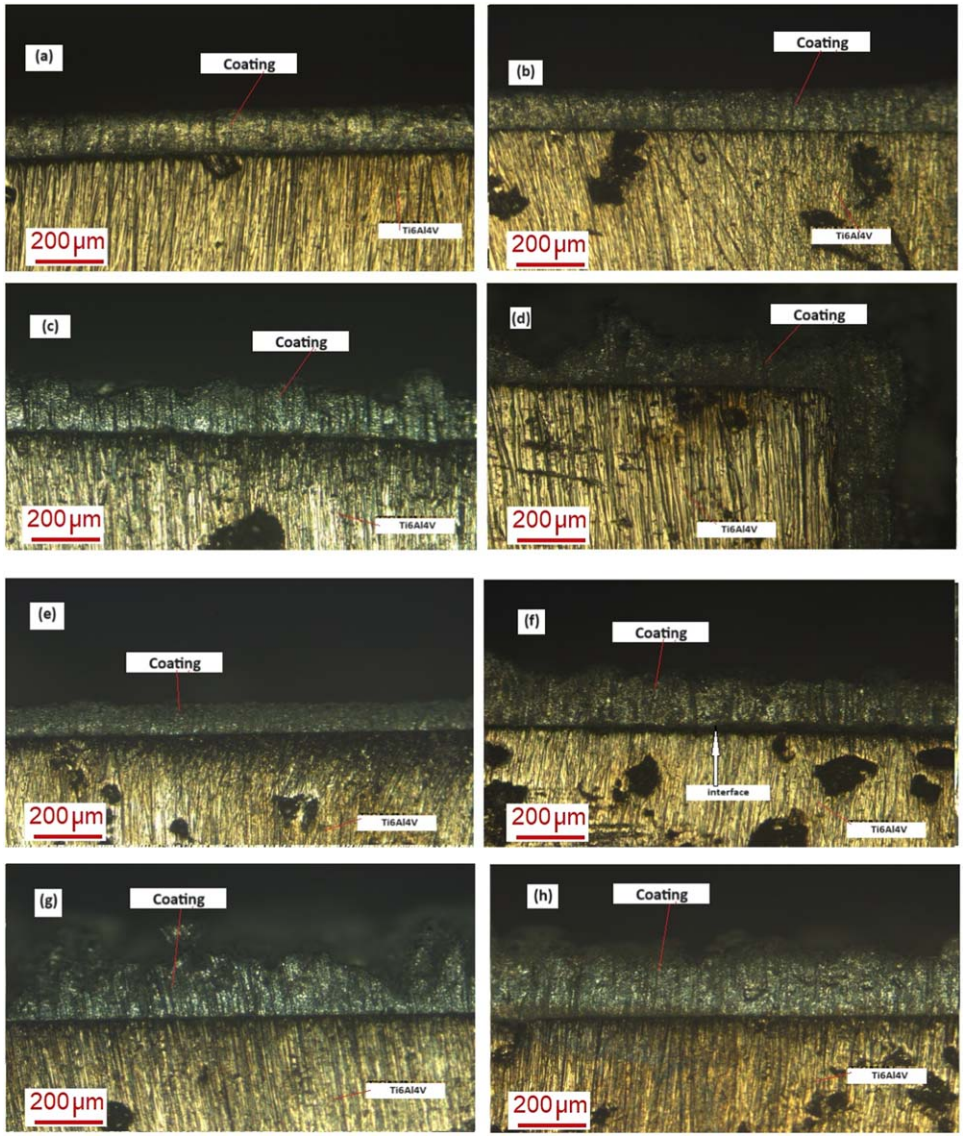


Figure 3. Optical microscope images of coating thicknesses (a) G30-5, (b) G60-5, (c) G30-10, (d) G60-10, (e) Z30-5, (f) Z60-5, (g) Z30-10, (h) Z60-10.

Table 4. EDS analysis values.

Sample number	TiO_2 addition amount (g/l)	Processing time (min.)	Anode	Ti Wt%	O Wt%	Zn Wt%
G30(5)	5	30		30,94	24,03	45,03
G60(5)	5	60		18,34	30,72	50,95
G30(10)	10	30	Graphite	4,92	28,33	66,75
G60(10)	10	60		14,83	17,85	67,32
Z30(5)	5	30		12,9	20,97	66,13
Z60(5)	5	60		20,03	23,7	56,1
Z30(10	10	30	Zinc	26,7	22,8	50,5
Z60(10)	10	60		37,9	24,3	37,8

3.2. Coating thickness

The images of the coating area taken with the optical metal microscope after all the test samples were coated are shown in figure 3, and the graph created according to the values of the approximate coating thickness measured during microscope imaging is shown in figure 4. Figure 5 shows an example of a cross-sectional EDS scan.

As shown in figures 3 and 4, a discernible pattern suggested that all samples' coating thickness increased as the amount of TiO_2 added increased. The specimens that underwent a 60-min treatment using a zinc anode and

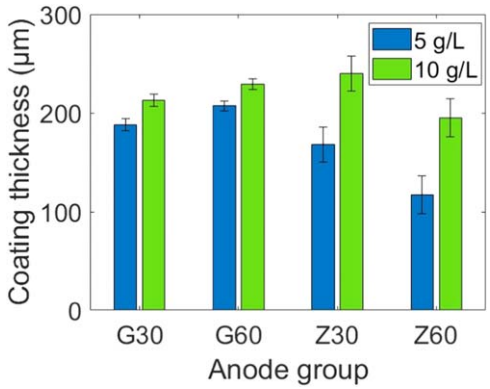


Figure 4. Average coating thickness values and cross-section image.

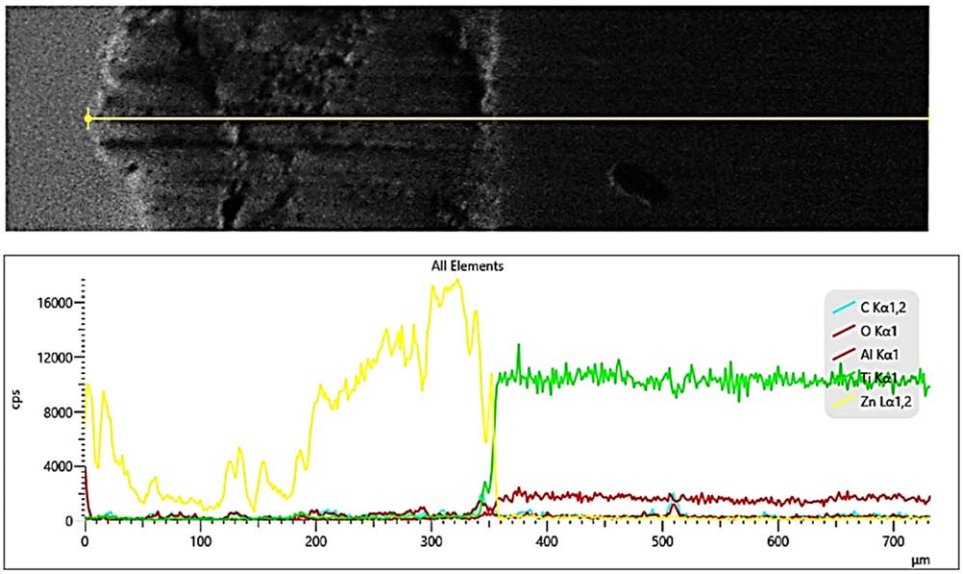


Figure 5. Cross-section EDS analysis example.

5 g l^{-1} TiO_2 demonstrated a minimum thickness of 117 μm for the coating. The samples that underwent treatment with a zinc anode and 10 g l^{-1} TiO_2 for 30 min exhibited a maximum coating thickness of 240 μm as measured. Conversely, the thickness of the coating increased directly and proportionally with the duration of the processing process when a graphite anode was employed. It is worth mentioning that an extended processing time has been found to decrease the coating thickness of zinc anodes.

3.3. Micro-hardness and wear resistance analysis

Figure 6 depicts Vickers hardness values corresponding to varying amounts of TiO_2 addition. The samples treated for 30 min with a graphite anode and 10 g l^{-1} particle addition exhibited the highest hardness value. Conversely, the samples treated for 30 min with a zinc anode and 5 g l^{-1} particle addition displayed the lowest hardness value. In their investigation of the microstructure-corrosion resistance relationship in Zn- TiO_2 nanocomposite coatings, Sajjadnejad *et al* [26] the introduction of additional TiO_2 particles creates new nucleation sites, leading to smaller particles and, consequently, an increase in hardness. A comparison of figure 5 and table 4 reveals that, in coatings produced with a Zn anode, the hardness value rises proportionally with both processing time and the quantity of additional particles.

The wear losses obtained from the wear tests are given in table 5. Figure 7 illustrates the variation in wear loss concerning the amount of TiO_2 addition. It was observed that with an increase in the quantity of additional particles in each process group, both hardness and wear loss exhibited an upward trend. The samples produced with the graphite anode, featuring the highest hardness value at 10 g l^{-1} addition and treated for 30 min (G30 (10)), displayed the most increased wear.

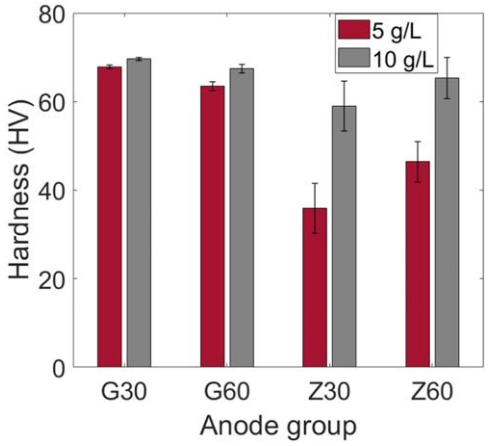


Figure 6. Hardness change according to TiO_2 addition amount.

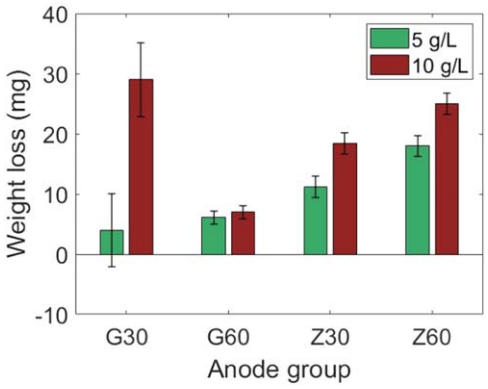


Figure 7. Wear loss change according to TiO_2 addition amount.

Table 5. Wear loss change.

	Addition amount (g/l)	Processing time (min.)	Anode	Mass loss (g)
G30(5)	5	30		0,004
G60(5)	5	60		0,0061
G30(10)	10	30	Graphite	0,029
G60(10)	10	60		0,007
Z30(5)	5	30		0,0112
Z60(5)	5	60		0,018
Z30(10)	10	30	Zinc	0,0184
Z60(10)	10	60		0,025

It is understood that the coating material, which becomes brittle with increasing hardness, moves away from the main structure more easily under the load applied in the wear tests. In addition, it can be stated that with increasing coating hardness, the adhesion at the coating interface and the base metal weakens. In this case, it became easier to separate the coating from the surface due to the increasing surface temperature due to the applied load and friction. Studies have reported that the wear mechanism is not only related to the hardness of the material but also that different parameters affect wear [27, 28]. A similar situation was encountered in the wear tests in this study. It has been observed that the hardness of the material has a decreasing effect on wear resistance, not increasing it.

Another issue that affects the amount of wear is the amount of porosity in the microstructure of the coating. When the surface morphologies in the microscope images in figure 2 and figure 3 are examined, it can be said

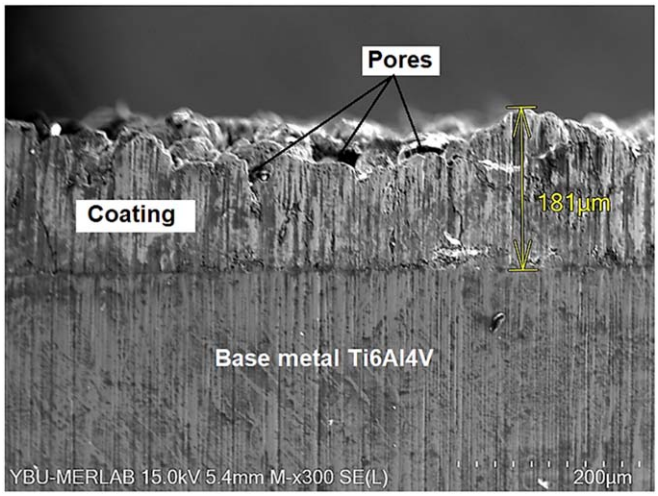


Figure 8. SEM image showing the microstructure of the coating region.

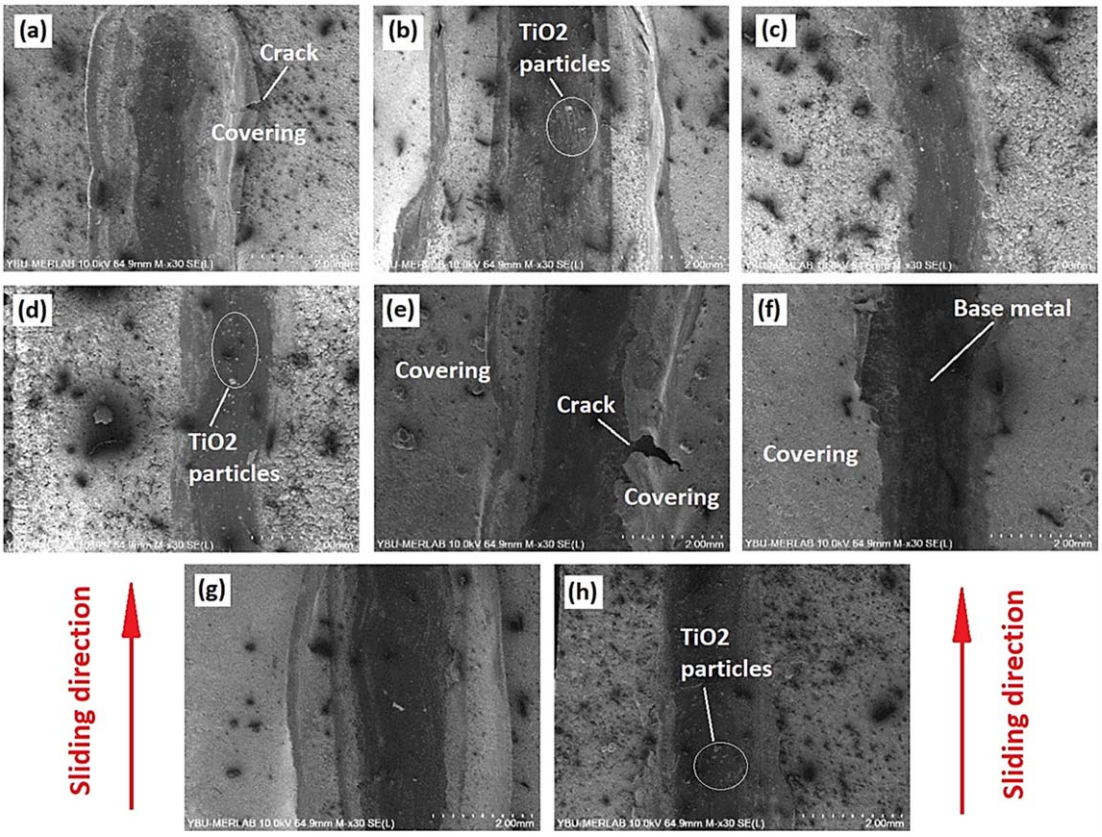


Figure 9. SEM images of wear path traces a) G30(5), b)G60(5), c)G30(10), d)G60(10), e)Z30(5), f)Z60(5), g)Z30(10)) and h)Z60(10).

that a very porous coating structure is formed. It is possible for the porous areas within the coating to be deformed much more easily and separated from the base metal during wear tests. The study conducted by Yılmaz and Buytoz reported that porosity affects hardness and wear resistance, and abrasive wear increases with increasing porosity [29]. Figure 8 shows the SEM image of the microstructure of the coating area. When looking at the SEM image, intense porosity and roughness, especially in the upper parts of the coating, attract attention.

In addition, TiO_2 particles in the structure were one of the factors affecting the wear behaviour. It is understood that TiO_2 particles in the very hard phase separate from the structure and emerge as a second corrosive agent. When the SEM images in figure 6 are scrutinized, it is evaluated that the TiO_2 particles separated

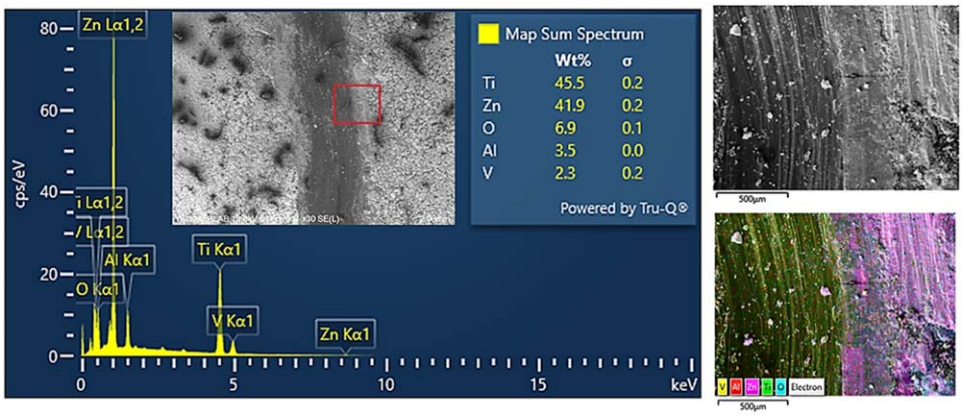


Figure 10. G30(10) wear path SEM and EDS examination.

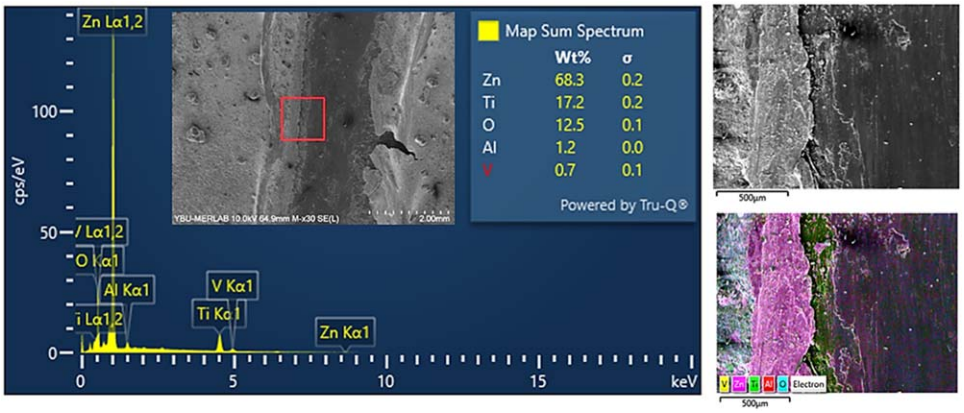


Figure 11. Z30(5) wear path SEM and EDS examination.

from the structure during the experiments got stuck between the steel test ball and the coating surface, acting like abrasive sandpaper grains, creating the abrasive wear mechanism. Singh *et al* reported that in three-body wear tests, the wear mechanism varies depending on the load, and material loss results from rolling the abrasive under smaller loads and micro-cutting under heavier loads. As a result, it is understood that factors other than hardness are effective on the wear behaviour of composites and that the subject needs to be examined from different aspects [30]. SEM images taken from worn surfaces are shown collectively in figure 9 to explore the wear behaviour in more detail.

SEM analyses, as depicted in figure 8, offered insights into the morphology of the wear marks. Wear/film patterns and wear scar images were acquired for each group. In the investigated groups, the worn surface exhibited expansion with lines aligned in the direction of movement and baffle separation in the worn area, indicative of a compressive wear mechanism [31]. Plastic deformation was observed along the wear scar, likely stemming from continuous contact pressure between the material surface and a harder body. Cracks beyond the worn region in the film were identified, aligning with findings reported by Alves *et al* [32]. This phenomenon could be attributed to film degradation resulting from fatigue wear and film delamination.

Figure 10 presents the SEM and EDS examination of the wear path for sample G30(10). Among the coatings fabricated with a zinc anode, minor wear was observed in sample Z30(5). SEM and EDS data analysis in figure 10 reveals that zinc adheres to the surface, providing a protective layer for the underlying base material.

When figures 10 and 11 are examined, it is understood that the oxygen element is included in the structure, and some oxide layer is formed on the surfaces. It is natural for this situation to occur in wear tests carried out in open atmospheric conditions. Therefore, one of the alloying elements in the base metal is aluminum, which is sensitive to oxygen and can react quickly. In the EDS analyses in figures 10 and 11, all alloying elements in the coating material Zn and the base metal Ti6Al4V alloy were also detected.

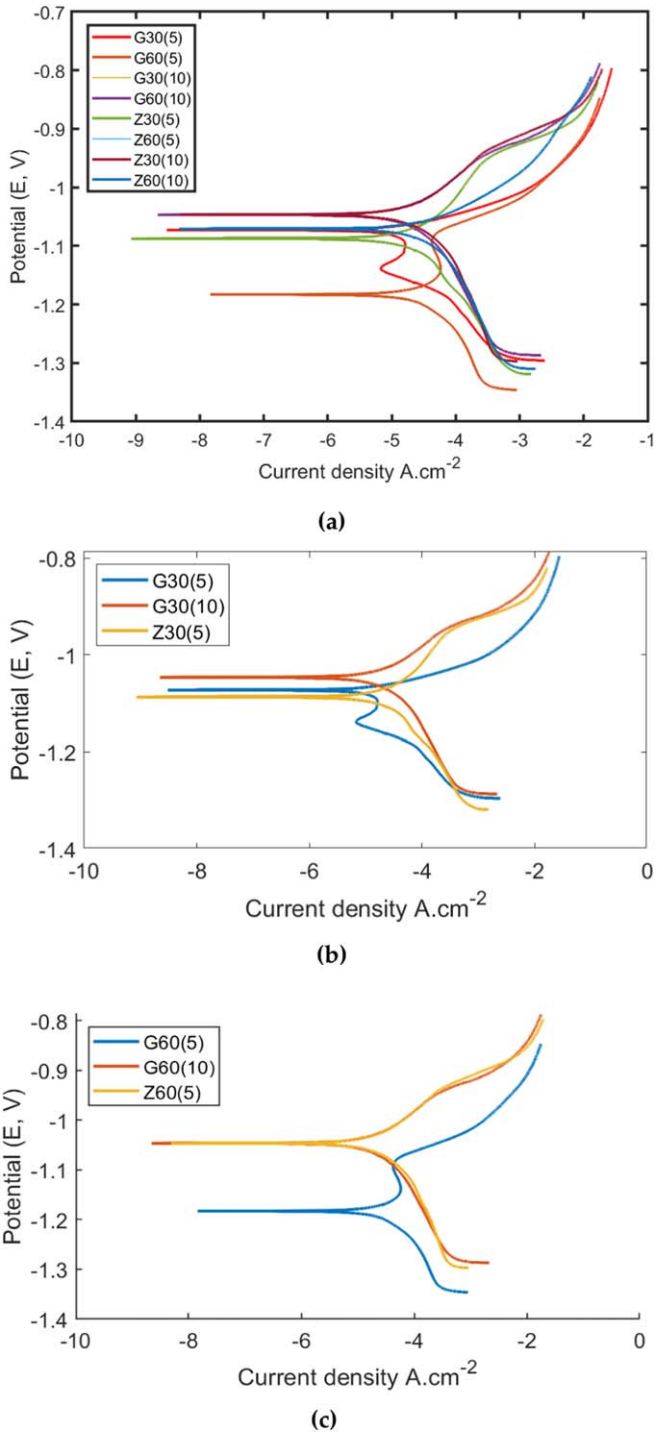


Figure 12. Potentiodynamic polarization curves (a) All samples, (b) samples G30-5, G30-10, Z30-5, (c) G60-5, G60-10, Z60-5.

3.4. Corrosion resistance

Figure 12 shows the potentiodynamic curves of TiO_2-doped Zn-supported coatings. Corrosion current density (i_{corr}), corrosion potentials (E_{corr}) and corrosion rate (mpy) values obtained from polarization curves are summarized in table 6. The lowest current density value was seen in samples processed for 30 min with 5 g l^{-1} TiO_2 added using graphite anode. When the corrosion potential values obtained from the polarization diagram were examined, the lowest corrosion potential was seen as −1.04 V. Samples with 10 g l^{-1} addition for 60 min using graphite anode, samples with 5 g l^{-1} addition for 60 min and 10 g l^{-1} for 30 min using zinc anode have the lowest corrosion potential. A lower corrosion potential indicates that the coating has lower chemical stability. This shows that the coatings protect the substrate with a galvanic cell. Barranco *et al* reported that zinc is preferentially solvated when zinc matrix coatings nucleate. One of the cathodic reactions for zinc coatings in an oxygen-containing solution is the reduction of dissolved oxygen. This process causes the pH on the coating

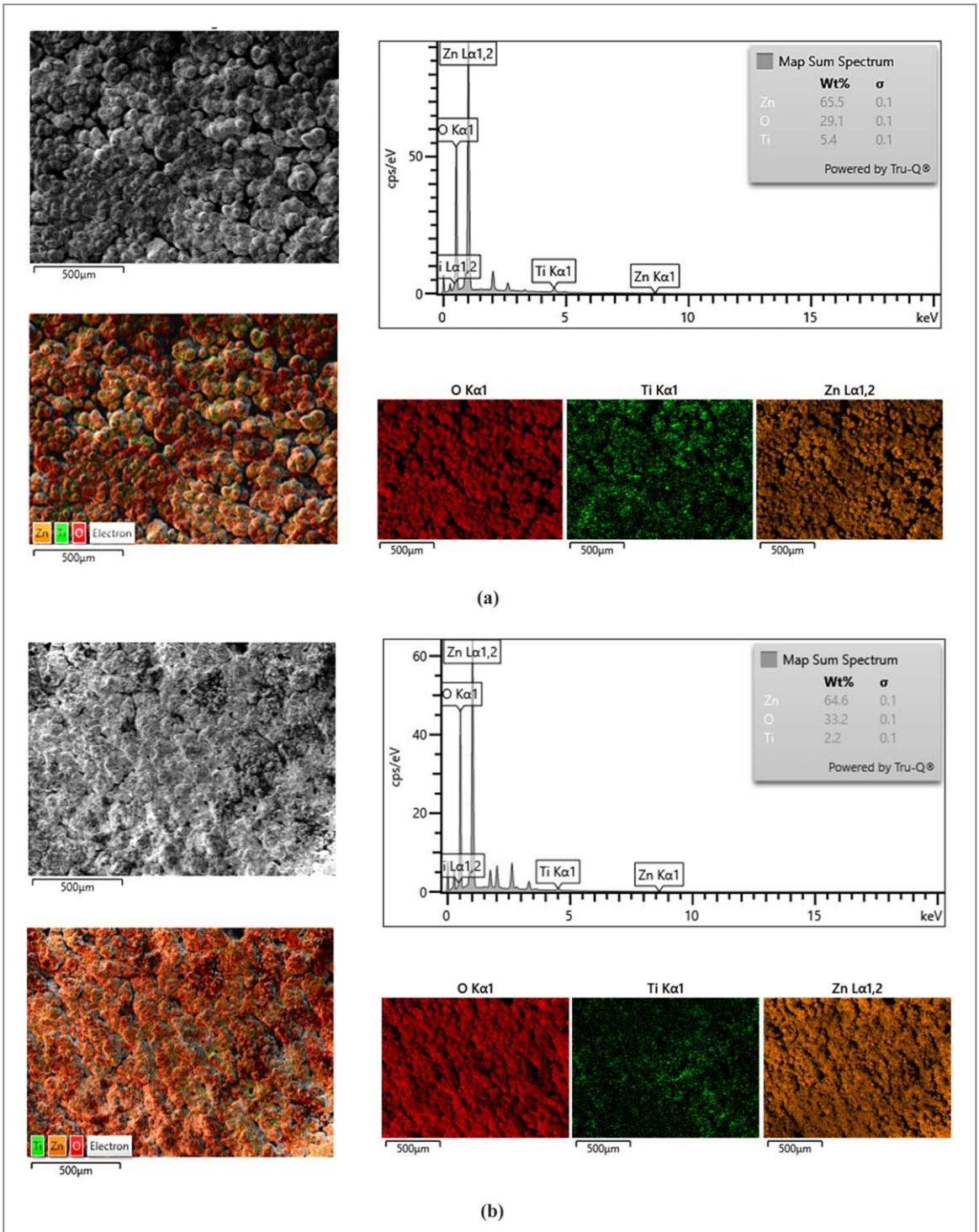


Figure 13. The SEM images and EDS map results ma de after the corrosion test in the simulated body fluid (SBF), (a) G30-10 (b) G60-10.

surface to increase locally, forming a thin and passive zinc-hydroxide layer. These hydroxide layers result in the formation of more corrosion products. However, due to the low solubility of corrosion products formed on the coating surface, the passive layer does not collapse, and therefore, the corrosion reaction occurs slowly [33]. Figure 13 and tables 6 and 7 show the summary of the SEM images and EDS map results made after the corrosion test in the SBF. As a result of the EDS examinations, the harmony of the presence of zinc and oxygen in the coating in the area exposed to corrosion and the fact that the substrate material is not exposed show that galvanic protection has been achieved. Grain boundaries are high-energy regions sensitive to electrochemical activities, and the coating is expected to show lower corrosion current density due to the larger crystallite size [21]. As seen in table 6, the lowest i_{corr} value was observed in the coating made with a graphite anode, which has a spherical and large grain structure.

Table 6. Potentiodynamic polarization values.

Sample No.	Anode	Process	i_{corr} (A/cm2) $\times 10^{-6}$	Ecorr (V)	βa (V/ decade)	βc (V/decade)	Corrosion Rate (mpy)
G30(5)	Garphite	5 g l^{-1} 30 min.	12,1	−1,07	3,08E-02	1,37E-01	4,19
G60(5)		5 g l^{-1} 60 min.	42	−1,18	8,05E-02	1,52E-01	14,41
G30(10)		10 g l^{-1} 30 min.	50,4	−1,06	6,66E-02	2,00E-01	17,32
G60(10)		10 g l^{-1} 60 min.	34,1	−1,04	1,12E-01	2,17E-01	11,7
Z30(5)	Zinc	5 g l^{-1} 30 min.	35,7	−1,09	1,39E-01	1,78E-01	12,27
Z60(5)		5 g l^{-1} 60 min.	44,7	−1,04	1,26E-01	2,46E-01	15,34
Z30(10		10 g l^{-1} 30 min.	27,9	−1,04	7,81E-02	2,38E-01	9,589
Z60(10)		10 g l^{-1} 60 min.	43,4	−1,07	6,84E-02	2,04E-01	14,91

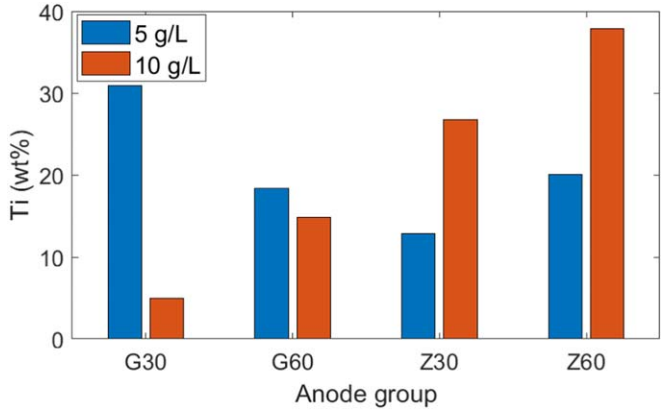


Figure 14. The EDS analysis results following the coating process indicate the weight percentage of Ti in the deposited coating on the surface.

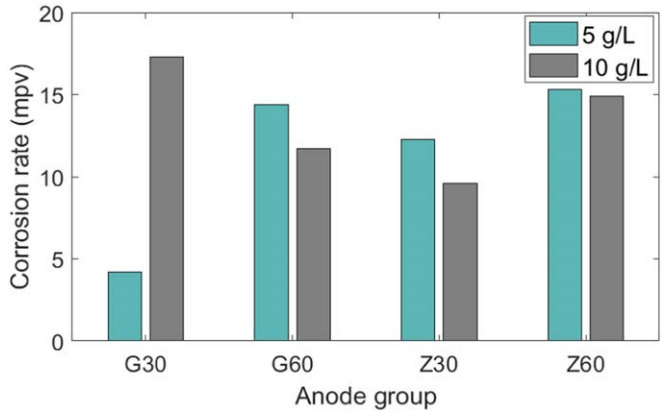


Figure 15. The variation in corrosion rate concerning the amount of TiO_2 addition.

Table 7. The EDS results obtained after the corrosion test in the simulated body fluid (SBF).

Sample number	TiO_2 addition amount (g/l)	Processing time (min.)	Anode	Ti Wt%	O Wt%	Zn Wt%
G30(5)	5	30	Graphite	7,43	28,74	63,83
G60(5)	5	60		10,38	23,88	65,8
G30(10)	10	30		5,42	29,13	65,45
G60(10)	10	60		9,7	27,22	63,08
Z30(5)	5	60	Zinc	1,88	33,42	64,7
Z60(5)	5	30		2,71	21,63	75,66
Z30(10	10	60		3,56	26,58	69,86
Z60(10)	10	30		2,23	33,21	64,56

Upon examination of the potentiodynamic curves, it was evident that the protection achieved by adding 10 $g\,l^{-1}$ when using a graphite anode for a 30-min processing time was equivalent to the protection attained by adding 5 $g\,l^{-1}$ when utilizing a zinc anode. Similarly, for a 60-min processing time, the values obtained by adding 10 $g\,l^{-1}$ using a graphite anode mirrored those achieved by adding 5 $g\,l^{-1}$ using a zinc anode.

Figures 14 and 15 show that the corrosion rate decreased as TiO_2 on the coating surface increased in the samples using zinc anode.

4. Conclusions

In the study, Ti6Al4V Grade 5 ELI samples were produced using a powder bed SLM method, and the TiO_2 ceramic material was coated homogeneously on these samples.

- The coating thickness increased with the incremental addition of TiO_2 in all samples. For those using graphite anode, the coating thickness increased directly to the processing time. However, in the case of Zn anodes, it has been established that an increase in processing time results in a decrease in coating thickness.
- It has been observed that the amount of wear increases and the corrosion rate decreases with the addition of TiO_2 in coatings made using zinc anode. The samples, produced with a graphite anode and treated for 30 min, exhibited the highest wear, particularly those with the highest hardness value at 10 g l^{-1} TiO_2 addition.
- As additional TiO_2 particles increased in each process group, hardness and wear loss demonstrated an upward trend.
- The coating material becomes brittle with increasing hardness and moves away from the main structure more easily under the load applied in the wear tests. In addition, it can be stated that with increasing coating hardness, the adhesion at the coating interface and the base metal weakens. In this case, it became easier to separate the coating from the surface due to the increasing surface temperature due to the applied load and friction. TiO_2 particles in the very hard phase are separated from the structure and act as a second abrasive, creating the abrasive wear mechanism.
- Additionally, it has been concluded that wear increases as the amount of porosity at the microstructure level in the coating increases. The lowest current density value and corrosion rate were seen in samples processed for 30 min with 5 g l^{-1} TiO_2 added using graphite anode. The corrosion potential was noted to be at its lowest in samples with higher i_{corr} values than others. Despite the seemingly rapid corrosion of zinc on the surface, the galvanic protection instigated by the formation of ZnOH contributes to increased corrosion resistance.

Data availability statement

The data cannot be made publicly available upon publication because no suitable repository exists for hosting data in this field of study. The data that support the findings of this study are available upon reasonable request from the authors.

Author contributions

Conceptualization, G K; methodology, G K, M K and M P; software, D K; validation, D Ö G; investigation, D Ö G; resources, M K and R C ; writing—original draft preparation, D Ö G; writing—review and editing, G K, M P, S S, E A N and R C; visualization, D K; supervision, G K.

All authors have read and agreed to the published version of the manuscript.

Funding

The authors extend their appreciation to King Saud University for funding this work through the Researchers Supporting Project number (RSP2024R164), King Saud University, Riyadh, Saudi Arabia. This article was co-funded by the European Union under the REFRESH—Research Excellence For Region Sustainability and High-tech Industries project number CZ.10.03.01/00/22_003/0000048 via the Operational Programme Just Transition and has been done in connection with project Students Grant Competition SP2024/087 'Specific Research of Sustainable Manufacturing Technologies' financed by the Ministry of Education, Youth and Sports and Faculty of Mechanical Engineering VŠB-TUO.

Institutional review board statement

Not applicable.

Conflicts of interest

The authors declare no conflict of interest.

ORCID iDs

Gökhan Küçüktürk https://orcid.org/0000-0002-2978-8968
Muharrem Pul https://orcid.org/0000-0002-0629-3516

Sachin Salunkhe https://orcid.org/0000-0001-6542-2050
Duran Kaya https://orcid.org/0000-0003-3102-9204

References

[1] Zhang L and Chen L 2019 A Review on biomedical titanium alloys: recent progress and prospect *Advanced Engineer Materials* **21** 1801215
[2] Kaur M and Singh K 2019 Review on titanium and titanium based alloys as biomaterials for orthopaedic applications *Mater. Sci. Eng.* C **102** 844–62
[3] Hao Y, Li S and Yang R 2016 Biomedical titanium alloys and their additive manufacturing *Rare Met.* **35** 661–71
[4] Li G, Chandra S, Rashid R A R, Palanisamy S and Ding S 2022 Machinability of additively manufactured titanium alloys: a comprehensive review *J. Manuf. Processes* **75** 72–99
[5] Mohammed M T 2018 Mechanical properties of SLM-titanium materials for biomedical applications: a review *Mater. Today Proc.* **5** 17906–13
[6] Khorasani A M, Gibson I, Goldberg M and Littlefair G 2016 A survey on mechanisms and critical parameters on solidification of selective laser melting during fabrication of Ti-6Al-4V prosthetic acetabular cup *Mater. Des.* **103** 348–55
[7] Li Y, Wong C, Xiong J, Hodgson P and Wen C 2010 Cytotoxicity of titanium and titanium alloying elements *J. Dent. Res.* **89** 493–7
[8] Costa B C, Tokuhara C K, Rocha L A, Oliveira R C, Lisboa-Filho P N and Pessoae J C 2019 Vanadium ionic species from degradation of Ti-6Al-4V metallic implants: *In vitro* cytotoxicity and speciation evaluation *Mater. Sci. Eng.* C **96** 730–9
[9] Segu D Z, Wang L L, Hwang P and Kang S W 2021 Experimental characterization of friction and wear behavior of textured Titanium alloy (Ti-6Al-4V) for enhanced tribological performance *Mater. Res. Express* **8** 8
[10] Shaikh S, Kedia S, Majumdar A G, Subramanian M and Sinha S 2020 45S5 bioactive glass coating on Ti6Al4V alloy using pulsed laser deposition technique *Mater. Res. Express* **6** 12
[11] Mansoor N S, Fattah-alhosseini A, Elmkhah H and Shishehian A 2020 Comparison of the mechanical properties and electrochemical behavior of TiN and CrN single-layer and CrN/TiN multi-layer coatings deposited by PVD method on a dental alloy *Mater. Res. Express* **6** 12
[12] Suresh V and Jegan A 2022 Experimental studies on wear and corrosion resistance of pulse electrodeposited Ni-TiO_2 nanocomposite coatings on AISI 304 stainless steel *Mater. Res. Express* **9** 12
[13] Moore B, Asadi E and Lewis G 2017 Deposition methods for microstructured and nanostructured coatings on metallic bone implants: a review *Adv. Mater. Sci. Eng.* **2017** 9
[14] Estrada-Cabrera A, Torres-Ferrer L R, Aztatzi-Aguilarbh O G, Vizcaya-Ruizb A D, Meraz-Rios M, Zarate-Triviñod D G and Arizmendi-Morquechoe A 2019 Chitosan-bioglass coatings on partially nanostructured anodized Ti-6Al-4V alloy for biomedical applications *Surf. Coat. Technol.* **375** 468–76
[15] Griesser H J 2016 Thin film coatings for biomaterials and biomedical applications *Woodhead Publishing Series in Biomaterials* 110 (Woodhead Publishing) 289–94
[16] Wang Y, Zhao S, Li G, Zhang S, Zhao R, Dong A and Zhang R 2020 Preparation and *in vitro* antibacterial properties of anodic coatings co-doped with Cu, Zn, and P on a Ti–6Al–4V alloy *Mater. Chem. Phys.* **241** 122360
[17] Zhang Z Y, Huang T Y, Zhai D J, Wang H B, Feng K Q and Xiang L 2023 Study on Zn-doped antibacterial bioactive coatings on Ti6Al4V titanium alloy surfaces by micro-arc oxidation *Surf. Coat. Technol.* **467** 129724
[18] Maniam K K and Paul S 2021 Corrosion performance of electrodeposited zinc and zinc-alloy coatings in marine environment *Corros. Mater. Degrad* **2** 163–89
[19] Wang R, He X, Gao Y, Zhang X, Yao X and Tang B 2017 Antimicrobial property, cytocompatibility and corrosion resistance of Zn-doped ZrO_2/TiO_2 coatings on Ti_6Al_4V implants *Mater. Sci. Eng.* C **75** 7–15
[20] He G, Lu S, Xu W, Yu T, Li J and Dai T 2018 Durable superhydrophobic Zn/ZnO/TiO_2 surfaces on Ti6Al4V substrate with self-cleaning property and switchable wettability *Ceram. Int.* **44** 638–47
[21] Mirak M, Alizadeh M, Ghaffari M and Ashtiani M N 2016 Characterization, mechanical properties and corrosion resistance of biocompatible Zn-HA/TiO_2 nanocomposite coatings *J. Mech. Behav. Biomed. Mater.* **62** 282–90
[22] Muresan L M 2016 Electrodeposited Zn-nanoparticles composite coatings for corrosion protection of steel *Handbook of Nanoelectrochemistry: Electrochemical Synthesis Methods, Properties, and Characterization Techniques* ed M Aliofkhazraei and A Makhlouf (Springer) 333–53
[23] Guan Q, Li Y, Bi X, Yang J, Zhou J, Li X, Cheng J, Wang Z, Wang B and Lu J 2019 Dendrite-free flexible fiber-shaped Zn battery with long cycle life in water and air *Adv. Energy Mater.* **9** 41
[24] Sajjadnejad M, Mozafari A, Omidvar H and Javanbakht M 2014 Preparation and corrosion resistance of pulse electrodeposited Zn and Zn–SiC nanocomposite coatings *Appl. Surf. Sci.* **300** 1–7
[25] Tuaweri T J and Wilcox G D 2006 Behaviour of Zn-SiO2 electrodeposition in the presence of N,N-dimethyldodecylamine *Surf. Coat. Technol.* **200** 5921–30
[26] Sajjadnejad M, Ghorbani M and Afshar A 2015 Microstructure-corrosion resistance relationship of direct and pulse current electrodeposited Zn-TiO_2 nanocomposite coatings *Ceram. Int.* **41** Part A 217–24
[27] Islak S and Çelik H 2015 Effect of Sintering temperature and boron carbide content on the wear behavior of hot pressed diamond cutting segments *Sci. Sinter.* **47** 131–43
[28] Cambronero L E G, Sánchez E, Ruiz-Roman J M and Ruiz-Prieto J M 2003 Mechanical characterisation of AA7015 aluminium alloy reinforced with ceramics *J. Mater. Process. Technol.* **143-144** 378–83
[29] Yılmaz O and Buytoz S 2001 Abrasive wear of Al_2O_3–reinforced aluminum–based MMCs *Compos. Sci. Technol.* **61** 2381–92
[30] Jiang Q C, Xu C L, Lu M and Wang H Y 2005 Effect of new Al–P–Ti–TiC–Y modifier on primary silicon in hypereutectic Al–Si alloys *Mater. Lett.* **59** 624–8
[31] Marquesa I S V, Alfaro M F, Cruz N C, Mesquita M F, Takoudis C, Sukotjo C, Mathew M T A V and Barao R 2016 Tribocorrosion behavior of biofunctional titanium oxide films produced by micro-arc oxidation: synergism and mechanisms *J. Mech. Behav. Biomed. Mater.* **60** 8–21
[32] Alves S A, Rossi A L, Ribeiro A R, Toptan F, Pinto A M, Celis J P, Shokuhfar T and Rocha L A 2017 Tribo-electrochemical behavior of bio-functionalized TiO_2 nanotubes in artificial saliva: understanding of degradation mechanisms *Wear* **384–385** 28–42
[33] Barranco V, Escudero M L and García-Alonso M C 2011 Influence of the microstructure and topography on the barrier properties of oxide scales generated on blasted Ti6Al4V surfaces *Acta Biomater.* **7** 2716–25